# Structure of pH-Dependent Block Copolymer Micelles: Charge and Ionic Strength Dependence

**Albert S. Lee,[†] Vural Bütün,[‡,§] M. Vamvakaki,[‡] Steven P. Armes,[‡] John A. Pople,[*,†] and Alice P. Gast[*,†,⊥]**

*Department of Chemical Engineering, Stanford University, Stanford, California 94305-5025, and School of Chemistry, Physics and Environmental Science, University of Sussex, Brighton BN1 9QJ, E. Sussex, UK*

*Received August 17, 2001*

ABSTRACT: We characterize the structures of various polyelectrolyte block copolymer micelles in dilute aqueous solution as a function of pH and ionic strength. The block copolymers carry a common core block, 2-(diethylamino)ethyl methacrylate (DEAEMA), and one of three coronal blocks, 2-(dimethylamino)ethyl methacrylate (DMAEMA), poly(ethylene oxide) (PEO), and DMAEMA, whose side chain amine groups are selectively quaternized with benzyl chloride (Q-DMAEMA). The PEO−DEAEMA, DMAEMA−DEAEMA, and Q-DMAEMA−DEAEMA copolymers form micelles with electrostatically neutral, weakly charged, and highly charged coronae, respectively. We adjust the fractional charge α on the DEAEMA and DMAEMA blocks by adjusting the solution pH. For DMAEMA−DEAEMA micelles increasing the fractional charge α swells the micelle corona while decreasing the aggregation number due to electrostatic repulsions. The decrease in aggregation number is also observed with increasing α for the PEO−DEAEMA and Q-DMAEMA−DEAEMA micelles, due to electrostatic repulsions between the hydrophobic DEAEMA blocks. Increasing the ionic strength causes the DMAEMA−DEAEMA micelle corona to shrink as the salt screens electrostatic repulsions within the corona. In all three copolymers increases in the ionic strength cause the micelle aggregation number to increase by screening the electrostatic repulsions between chains. Trends in the corona thickness with varying fractional charge and ionic strength are compared with a number of theoretical models providing additional insight into the micelle structure.

## 1. Introduction

Amphiphilic block copolymers have been a subject of much technological and scientific interest because of their interesting solution properties. One of their interesting properties is their associative behavior, where the insoluble parts coalesce to minimize their contact with the solvent and the molecules aggregate to form micelles. The insoluble blocks aggregate to form a dense core, and the soluble blocks extend out into the solvent to form a corona.[1,2] These micelles can assume various shapes, ranging from wormlike to spherical micelles.[3,4] The behavior of uncharged diblock copolymers is fairly well understood experimentally and theoretically in terms of their structure and micellar associative behavior.[5−17]

More recently, theoretical models describing the structure of charged polyelectrolyte micelles have been increasing. Many of the theories describe spherical micelles with a charged corona and an electrostatically neutral core.[18−29] While the theories for neutral micelles draw from analogies with semidilute polymer solutions, semidilute polyelectrolyte theory is not as well established, and the charged micelles are more difficult to model. A spherical micelle can be thought of as a polymer brush at a curved interface, where polymer chains are end-grafted at a solid−liquid interface, and models of charged polymer brushes at a flat interface offer additional insight into the structure of the charged micelle corona. Theories for both micelles and polymer brushes have been developed for so-called quenched polyelectrolytes where the charges are fixed along the polymer chain,[18−26] as well as for annealed systems where the charge distribution is allowed to vary along the polymer chain, as in a weak polyacid or polybase.[26−29]

While the number of theories has been increasing, the experimental studies have shown some interesting trends. For both quenched and annealed polyelectrolyte micelles as well as brushes, the addition of salt is found to screen electrostatic interactions in the micelle corona or brush to cause the thickness to decrease.[25,30−36] Addition of salt also promotes larger micellar aggregation numbers or polymer brushes with higher grafting densities because of electrostatic screening of repulsions between chains.[30,33,37] For the annealed polyelectrolyte micelles and brushes the pH controls the degree of charge in the micelle corona or polymer brush and can induce swelling due to electrostatic repulsions.[35,37−40]

One specific class of polyelectrolyte micelles are pH-sensitive micelles where the copolymers aggregate to form micelles when the pH is adjusted beyond the critical value.[41,42] In general, aqueous copolymer systems have been difficult to prepare and to work with, often requiring a cosolvent such as methanol or THF to adequately dissolve the polymers to form relatively stable, uniform micelles.[43] In contrast, the pH-sensitive copolymers can be dissolved as unimers by adjusting the pH and then slowly titrated to form relatively uniform micelles without the use of a cosolvent. The associative behavior of neutral copolymers has traditionally been characterized by the critical micelle concentration, or cmc, and these pH-sensitive copolymers can in addition be characterized by the critical pH

[†] Stanford University and Stanford Synchrotron Radiation Laboratory.
[‡] University of Sussex.
[§] Current address: Faculty of Arts and Science, Department of Chemistry, Osmangazi University, 26480, Eskisehir, Turkey.
[⊥] Current address: Department of Chemical Engineering, Massachusetts Institute of Technology, Cambridge, MA, 02139.
* To whom correspondence should be addressed.

10.1021/ma0114842 CCC: $22.00 
Published on Web 09/28/2002

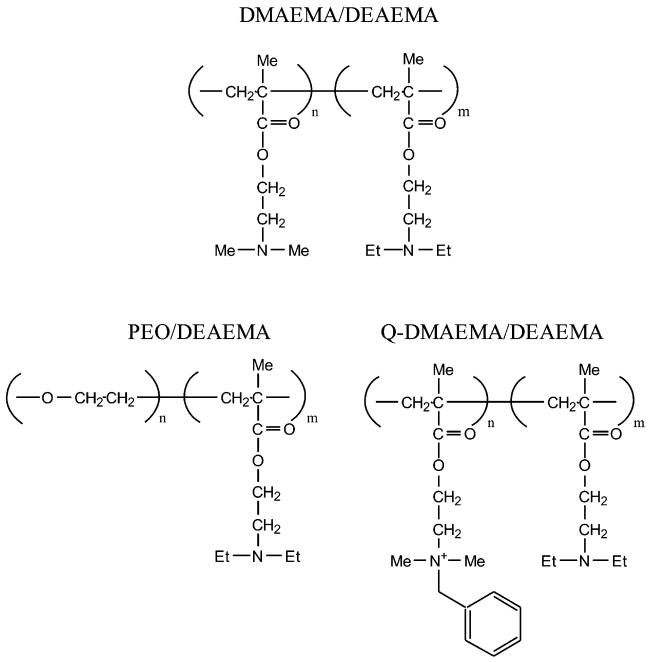


**Figure 1.** Chemical structures of the novel pH-sensitive copolymers studied in this work.

denoted pH* or the critical fractional charge α* where the copolymer fractional charge α depends on the pH and takes values $0 \leq \alpha \leq 1$. Another interesting aspect of the pH sensitivity is that these copolymers could serve as a model for a delivery system, where the solute encapsulated in the micelle cores is released as the micelles break apart when they reach a target pH. The pH-induced release of a solute is potentially useful in drug delivery[41,44−46] or environmental remediation systems.[47]

Recently, Armes and co-workers[48−51] have developed a series of novel pH-sensitive block copolymers which form micelles having coronae with various electrostatic properties. Among these novel block copolymers are 2-(dimethylamino)ethyl methacrylate-*block*-2-(diethylamino)ethyl methacrylate (DMAEMA−DEAEMA), poly(ethylene oxide)-*block*-2-(diethylamino)ethyl methacrylate (PEO−DEAEMA), and DMAEMA−DEAEMA with the DMAEMA block selectively quaternized with benzyl chloride (Q-DMAEMA−DEAEMA). The three copolymers contain the same hydrophobic DEAEMA block, and their chemical structures are shown in Figure 1. Under acidic conditions, the amine groups on the DEAEMA side chains are protonated, causing the copolymers to become hydrophilic and to remain as unimers in solution. The subsequent addition of base deprotonates the side chains, causing the DEAEMA block to become hydrophobic. Above the critical pH the copolymers aggregate to form micelles. The DEAEMA block forms the micelle core while the hydrophilic DMAEMA, PEO, or Q-DMAEMA block extends into the solvent to form the micelle corona. The primary difference between the three copolymers is in the electrostatic properties of the hydrophilic block forming the micelle corona, where we have electrostatically neutral, weakly charged, and strongly charged hydrophilic blocks from PEO, DMAEMA, and Q-DMAEMA, respectively. An interesting aspect of the DMAEMA−DEAEMA micelles is that the fractional charge α on the DMAEMA block can be varied by adjusting the solution pH, such that the degree of charge in the micelle corona can be varied. The DMAEMA block acts as a weak polybase and forms a micelle corona expected to behave as an annealed brush, whereas in Q-DMAEMA−DEAEMA the charges are fixed and the coronal chains are quenched polyelectrolytes.

In this work we seek to study these three copolymers to further the understanding of polyelectrolyte block copolymer micelles with varying pH and ionic strength. To our knowledge, a unique aspect of this work is that we study the charge dependence not only of the hydrophilic coronal block but also of the hydrophobic core block. In addition, there have been few attempts in the literature[25,36,39,40,52] to directly compare experimental results with theoretical models for polyelectrolyte micelles and brushes, and our work contributes toward filling this gap.

## 2. Theoretical Models

**2.1. Electrostatically Neutral Micelles.** Electrostatically neutral micelles are significantly easier to model than charged micelles, and a range of mean field and self-consistent-field models have been developed which describe their structure. The starlike micelle scaling model based on the work of Daoud and Cotton[11] and developed by others[6,17] describes the micelle as a spherical core surrounded by a shell of chains extending out into the solvent, as in a star, shown in Figure 2a. The model depicts the coronal shell as a series of connected blobs whose sizes increase with increasing distance $r$ away from the core.

**2.2. Quenched Polyelectrolytes.** A number of mean-field and self-consistent-field models as well as scaling models have been developed to describe quenched polyelectrolyte brushes at both planar and curved interfaces. Some of these models describe the brushes in the salted regime, where added salt is present, while others describe the brushes in the osmotic regime, where there is no added salt. Several of these models describing quenched polyelectrolyte brushes are summarized in Table 1, where the brush height $L$ dependence on ionic strength $C_s$ and fractional charge α are given. Other important parameters governing $L$ are the statistical segment length in the brush $a$, the number of statistical segments per chain $N$, and the grafting density $\sigma$. Two other important parameters in polyelectrolyte systems are the Bjerrum length $l_b$ defined as $l_b = e^2/4\pi\epsilon k_B T$, where $e$ is the electron charge and $\epsilon$ is the solvent dielectric constant. The Debye screening length $\kappa^{-1} = (8\pi l_b C_s z^2 N_A)^{-1/2}$ describes the electrostatic screening due to the presence of ions where $z$ is the valency of the ions and $N_A$ is Avogadro's constant. In the case of micelles, the number of chains per micelle $f$ and the micelle core radius $R_c$ are also important parameters influencing $L$. Also, in the case of micelles, $N_c$ and $N_s$ are the number of segments per block copolymer chain for the core and corona, respectively.

Zhulina and Borisov describe an osmotic brush regime, where the charge density is high, such that most of the counterions are found within the brush where they can cause an osmotic force balanced by an elastic force.[26] In this description for quenched polyelectrolytes, the coronal shell can be described as a series of electrostatic blobs with a constant blob size. As shown in Figure 2b, these electrostatic blobs are not necessarily touching between chains, in contrast with the starlike micelle model. An inner region of the micelle corona is also described where the blobs are packed as in the

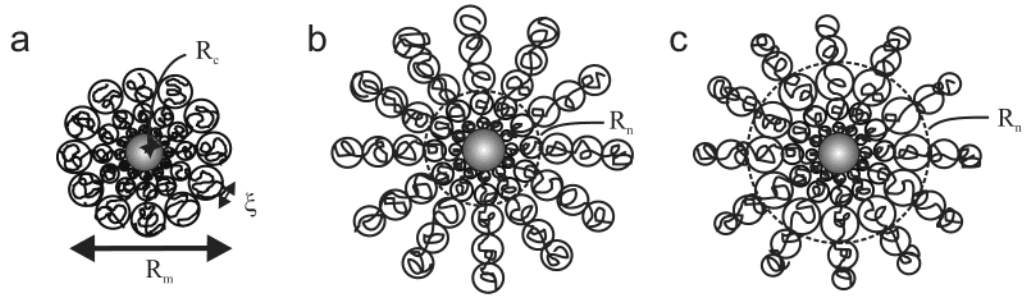


**Figure 2.** Cartoons of the (a) starlike micelle, (b) micelle with a charge-quenched corona, and (c) micelle with a charge-annealed corona.

**Table 1. Summary of Model Predictions: Quenched Brushes**

| ref | predicted thickness $L$ | geometry | salt |
|---|---|---|---|
| | Ionic Strength Dependences | | |
| 20 | $L \sim N(a^2\sigma)^{1/3}C_s^{-2/3}$ | plane | salted |
| 21 | $L \sim aN_s^{3/5}f^{1/5}/(a^3C_s)^{2/5}$ | sphere | salted |
| 25 | | | |
| 74 | | | |
| 75 | $L \sim \sigma^{1/3}C_s^{-1/2}$ | plane | salted |
| 25 | $L \sim \sigma^{1/3}C_s^{-1/6}$ | plane | salted |
| 25 | $L \sim R_c^{2/5}\sigma^{1/5}C_s^{-1/10}$ | sphere | salted |
| 19 | $L \sim Na\sigma^{1/3}(aC_s)^{-1/3}$ | plane | salted |
| | Fractional Charge α Dependences | | |
| 19, 26, 28 | | | |
| 27 | $L \sim \alpha^{1/2}Na$ | sphere/plane | osmotic |
| 23 | $L \sim N_s(l_b/a)^{2/7}\alpha^{4/7}a$ | sphere | osmotic |
| 72 | $L \sim N^{3/5}f^{1/5}\alpha^{2/5}(C_sa^3)^{-1/5}a$ | sphere | salted |

starlike micelle model, and its boundary $R_n$ occurs where the concentration of segments in the packed blob equals that of the electrostatic blob.

**2.3. Annealed Polyelectrolytes.** The case of annealed polyelectrolytes is much more complicated than the quenched case. For brushes composed of weak polyacids or polybases the charges along the polymer chains are allowed to anneal to adjust to the local acid or base concentrations. This annealing causes the charge distribution in the brush to vary with distance from the grafting interface. A number of theories for annealed brushes are summarized in Table 2. The theories describe annealed brushes at planar and spherical interfaces under various ionic conditions. In the case of annealed brushes, the fractional charge of the polymer in bulk solution $\alpha_b$, the $H^+$ concentration in bulk solution $C_H$*, and the acid or base dissociation constant $K$ of the polyelectrolyte are important.

Zhulina and Borisov[26] extended their model for quenched polyelectrolyte brushes described in the previous section to describe weak polyacid brushes. The treatment assumes no salt added such that all ions are $H^+$ ions. If the electrostatic blobs are defined such that each blob contains one charge, the blob size is predicted to decrease with distance from the core as the number of charges increases. Zhulina and Borisov also describe an internal sublayer, and their description of the annealed micelle corona is depicted in Figure 2c.

**2.4. Starlike Micelle Model with Electrostatic Blobs.** We extend the starlike micelle model for polyelectrolyte micelles by incorporating the concept of an electrostatic blob in the description of the coronal shell. We assume in this treatment that the charges are distributed evenly along the chains. Borisov[22] and Zhulina and Borisov[26] describe an electrostatic blob occurring at large aggregation numbers where most of the counterions remain in the corona and dominate the swelling. In this case the blob size is constrained such that there is one charge in each blob, so that the number of segments per blob $N_\xi$ is $\alpha^{-1}$. These electrostatic blobs are each the same size, as depicted in Figure 2b. Describing the blobs to exhibit the Flory scaling $\xi = N_\xi{}^\nu a$, the electrostatic blob size becomes $\xi_e = \alpha^{-\nu}a$ and the corona thickness is simply the sum of $\alpha N$ blobs

$$L = \alpha^{1-\nu}Na \tag{1}$$

For $\nu = {}^1/_2$, eq 1 is the same as the $L \sim \alpha^{1/2}Na$ scaling found by Pincus in his mean-field analysis.[19] The blob analysis shows that the constant of proportionality for Pincus' $L \sim \alpha^{1/2}Na$ scaling is approximately 1. We can add the predicted corona thickness with the predicted core radius from the starlike micelle model to obtain a model for the overall micelle size $R_m$

$$R_m = \left(\frac{3N_cf}{4\pi\rho_c}\right)^{1/3} + \alpha^{1/2}Na \tag{2}$$

for $\nu = {}^1/_2$. We integrate the density profile for the corona containing electrostatic blobs, $\rho_e = \alpha^{\nu-1}f\ /4\pi ar^2$ to determine $R_g$.

## 3. Experimental Methods

**3.1. Materials.** Block copolymers of 2-(dimethylamino)ethyl methacrylate-*block*-2-(diethylamino)ethyl methacrylate (DMAEMA−DEAEMA) and poly(ethylene oxide)-*block*-2-(diethylamino)ethyl methacrylate (PEO−DEAEMA) were synthesized at Sussex. The details of the synthesis are reported elsewhere.[48,49] A third copolymer sample (Q-DMAEMA−DEAEMA) was produced at Sussex by selectively quaternizing the DMAEMA amine groups in the DMAEMA−DEAEMA copolymer with benzyl chloride. DMAEMA and DEAEMA homopolymers were also synthesized, and PEO homopolymer was purchased from Polysciences. In addition, a bet-DMAEMA homopolymer was synthesized, where the DMAEMA homopolymer was betainized using propane-1,3-sultone.[48,50] The copolymer and homopolymer properties are listed in Table 3.

Gel permeation chromatography was used to measure molecular weights and polydispersity, except for the case of Q-DMAEMA−DEAEMA, where the molecular weight was calculated from the NMR data showing 100% quaternization of the DMAEMA block. NMR measurements were also used to determine the relative mole fractions of each block. The solid-state density of DEAEMA homopolymer, 1.046 g/mL, was measured with helium pycnometry.

We prepared each sample by dissolving the copolymer in Milli-Q deionized water with enough HCl to match the monomer concentration of amine groups. In this way, complete molecular dissolution of the copolymers is ensured. Copolymer concentrations range from 0.001 to 0.01 g/mL. The copolymer solutions are filtered through either a 0.2 $\mu$ Whatman Anotop or 0.45 $\mu$ Gelman Nylon syringe filter before micelle formation. In the case of Q-DMAEMA−DEAEMA, aggregates are detected via light scattering even at low pH, and a series of

**Table 2. Summary of Model Predictions: Annealed Brushes**

| investigators | predicted thickness $L$ | geometry | salt |
|---|---|---|---|
| Zhulina et al.[28] | $L \sim Na^{4/3}\sigma^{-1/3}[(\alpha_b/(1-\alpha_b)(C_H^* + C_s)]^{1/3}$ | plane | osmotic |
| Zhulina et al.[28] | $L \sim N(a^2\alpha^2\sigma C_s^{-1})^{1/3}$ | plane | salted |
| Lyatskaya et al.[29] | $L \sim Na[-\ln(1-\alpha_b) - \alpha_0]^{1/2}$ $\alpha_0 \sim \{(1/\sqrt{6})[(2+\pi)/2\pi][a^3(C_H^* + C_s)/a^2\sigma][\alpha_b/(1-\alpha_b)]\}^{2/3}$ | plane | osmotic |
| Lyatskaya et al.[29] | $L \sim Na\{(2/\pi^2)a^2\sigma[\alpha_b^2/a^3(C_H^* + C_s)]\}^{1/3}$ | plane | salted |
| Zhulina et al.[26] | $L \sim aN_s^3(Ka^3)/\sigma R_c^2$ | sphere | osmotic |
| Borisov and Zhulina[72] | $L \sim N^3\alpha_b f^{-1}(C_H^* + C_s)a^4$ | sphere | salted |

**Table 3. Copolymer and Homopolymer Properties**

| sample | mol wt | $M_w/M_n$ | A units | B units |
|---|---|---|---|---|
| DMAEMA−DEAEMA | 32 600 | 1.10 | 97 | 94 |
| PEO−DEAEMA | 8 300 | 1.33 | 45 | 34 |
| Q-DMAEMA−DEAEMA | 44 900 | | 97 | 94 |
| DEAEMA homopolymer | 15 000 | 1.06 | | 81 |
| DMAEMA homopolymer | 12 300 | 1.08 | 78 | |
| PEO homopolymer | 1 470 | 1.05 | 33 | |
| bet-DMAEMA homopolymer | 22 350 | 1.14 | 80 | |

filtrations were required to minimize these aggregates. The Q-DMAEMA−DEAEMA solutions were first filtered through 0.45 $\mu$ Gelman Nylon and 0.1 $\mu$ Whatman Anotop syringe filters. These filtered solutions were then ultrafiltered using Millipore Ultrafree-CL 300 000 NMWL filters at 1700 rpm (480 G) in a Beckman GPR centrifuge for 3.5 h. Prior to ultrafiltration of the Q-DMAEMA−DEAEMA solutions, pure water was flushed through the filters.

For the titrations, standardized acid and base solutions of HCl and KOH were each prepared at 1 and 0.1 M concentrations. The dissolved copolymer solutions were slowly titrated to higher pH using KOH and gently agitated or left to equilibrate overnight before experiments were performed.

**3.2. Potentiometric Titrations.** A Rainin motorized pipet (EDP Plus) with a 100 $\mu$L liquid end was used to deliver known amounts of standardized HCl or KOH to the samples while the pH was monitored on an Orion 611 pH meter with a semimicrocombination electrode (Orion Ross 8103). Because of the tendency of the pH to drift over many minutes, the accuracy of the pH is estimated to be approximately 0.05 pH units. Titration curves were generated by first titrating the solution to low pH with 1 M HCl to ensure complete dissolution of the copolymer and then measuring the pH in 10−100 $\mu$L increments of 0.85 or 0.085 M KOH.

As HCl and KOH are added during the titrations, $K^+$ and $Cl^-$ ions are unavoidably added. The effective amount of KCl added during the titrations is taken into account for salt-dependent measurements. During polymer dissolutions, just enough HCl is added to protonate all the amine groups, ensuring complete dissolution and minimizing the amount of effective KCl added; thus, solutions with lower polymer concentrations have lower background ionic strengths.

We define $\alpha$ as the ratio $C_H/C_m$, where $C_H$ is the effective concentration of added HCl and $C_m$ is the monomeric concentration of polymer chains. When defined in this way, $\alpha$ approximates the degree of protonation, or the fraction of amine groups in the chain protonated, assuming that all the added protons protonate the amine groups. This definition of $\alpha$ also assumes that the fractional charge inside the micelle corona is the same as that of the copolymer in bulk solution: $\alpha \sim \alpha_b$. In some cases the calculations for $C_H$ needed to be adjusted to cause the $\alpha = 0$ and $\alpha = 1$ values to occur at the inflections of the titration curves. We define $\alpha^*$ as the critical $\alpha$, below which micelles form.

We can model the titration of the copolymer solution as the titration of a monoprotic weak acid buffer with a strong base, where the copolymer comprises monomers having an average p$K_a$. Using average p$K_a$ values obtained from the titrations described above, model titration curves can be calculated from simple acid−base equilibrium equations.[53] Titration curves of DMAEMA−DEAEMA, PEO−DEAEMA, and Q-DMAEMA−DEAEMA copolymers are shown in Figure 3, along with the calculated titration curves for p$K_a$ values of 7.2, 6.8, and 7.1 for the three copolymers, respectively. The varying ionic

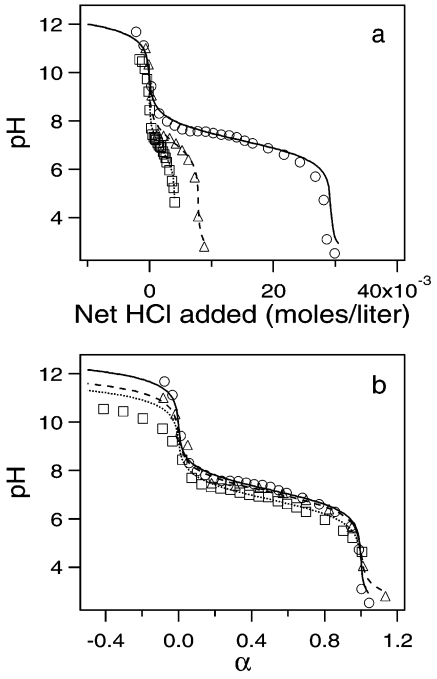


**Figure 3.** Titration curves for DMAEMA−DEAEMA (○), PEO−DEAEMA (□), and Q-DMAEMA−DEAEMA (△) copolymers. Lines are model calculations.

conditions and difference between the DMAEMA and DEAEMA p$K_a$ are responsible for the slight differences between the three copolymer p$K_a$ values. The PEO−DEAEMA and Q-DMAEMA−DEAEMA micelles remain in solution even at high pH. The model and experimental titration curves as a function of $\alpha$ are shown in Figure 3b. The regions where $\alpha < 0$ or $\alpha > 1$ are where the acid or base concentration exceeds that required to fully deprotonate or fully protonate the chain. Good agreement between the model calculations and the measured data validates our assumption that effectively all of the $H^+$ ions from the added HCl protonate the amine groups.

**3.3. Light Scattering Measurements.** Light scattering measurements were conducted by shining a laser through copolymer solutions and measuring the scattered light intensity at 90° relative to the incident beam. A fiber optic couples the light to the photomultiplier tube (PMT), where the light intensity is recorded by a Brookhaven Instruments BI-9000 correlator. Upon the onset of micelle formation at pH* and $\alpha^*$, the scattered intensity significantly increases. Certain regions of the intensity vs $\alpha$ curves are linear, allowing extrapolation to the baseline to obtain $\alpha^*$. As seen in Figure 4, $\alpha^*$ increases with the ionic strength due to screening of electrostatic repulsions, allowing micelles to form at higher fractional charge $\alpha$. In our studies of the micelle structure, we remain below the $\alpha^*$ curves in Figure 4 such that we observe the charge and ionic strength dependence without inducing micelle breakup.

**3.4. Dynamic Light Scattering.** Dynamic light scattering (DLS) measurements were performed as described in more detail elsewhere.[42] Data were collected over a duration ranging from 4 to 30 min and stored and processed on a Brookhaven Instruments BI-9000 correlator. In converting from an intensity autocorrelation to an electric field correlation, the corr-

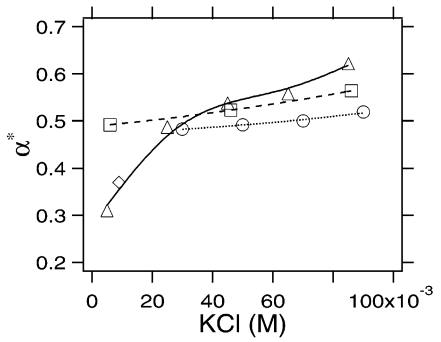


**Figure 4.** Critical fractional charge α* for micelle formation with varying salt concentration. Values are shown for 0.001 g/mL (□) and 0.005 g/mL (○) DMAEMA−DEAEMA and 0.001 g/mL PEO−DEAEMA (△) copolymers. Also shown is a measurement for 0.004 g/mL Q-DMAEMA−DEAEMA (◇). Lines are interpolations to guide the eye.

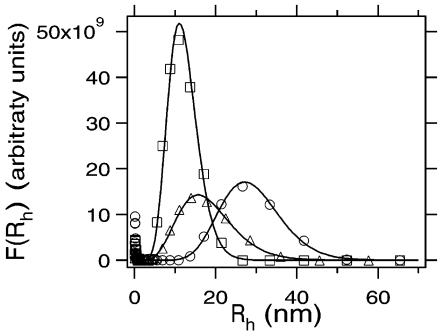


**Figure 5.** Representative DLS CONTIN size distributions for DMAEMA−DEAEMA (○), PEO−DEAEMA (□), and Q-DMAEMA−DEAEMA (△) micelles. Lines are fits to a theoretical Schulz distribution to obtain polydispersities.

elator calculates the baseline $\langle I(t)\rangle^2$ and also measures the baseline at long delay times $\tau$. The measured and calculated baselines are typically within 0.2% for our copolymer/micelle solutions. For dilute, monodisperse particles the autocorrelation function $g^{(1)}(\mathbf{q},\tau)$ is an exponential decay $g^{(1)}(\mathbf{q},\tau) = e^{-q^2 D_0 \tau}$ where the self-diffusion coefficient $D_0$ is related to the particle hydrodynamic size $R_h$ and viscosity $\mu$ by the Stokes−Einstein equation $D_0 = k_B T/6\pi\mu R_h$.

For a system with a distribution of sizes the autocorrelation function $g^{(1)}(\mathbf{q},\tau)$ takes the form[54]

$$g^{(1)}(\mathbf{q},\tau) = \int_0^\infty F(R_h) \exp\left[-\frac{q^2 k_B T}{6\pi\mu} R_h^{-1}\tau\right] dR_h + \Delta \quad (3)$$

with a distribution of exponential decays. Scattering from large impurities such as dust contributes to the autocorrelation function as an additive "dust term" Δ. The filtered samples were generally dust-free, and the dust term was usually well below 0.01 or it was disregarded. The autocorrelation data were analyzed using CONTIN,[55] a FORTRAN program producing an optimum $F(R_h)$ size distribution via a constrained Laplace transform of the data. The optimum smoothing to fit the data called for a "probability to reject" of 0.4. We report the average of 3−5 measurements at a 90° scattering angle; individual measurements at other scattering angles confirmed these results.

Shown in Figure 5 are representative CONTIN distributions for each of the copolymer micelles, where the experimental results shown by the markers are averages over five repeated measurements. The solid lines in Figure 5 are Schulz distribution[56] fits of the distributions, yielding fractional standard deviations of 0.26, 0.30, and 0.37 for the DMAEMA−DEAEMA, PEO−DEAEMA, and Q-DMAEMA−DEAEMA micelles, respectively.

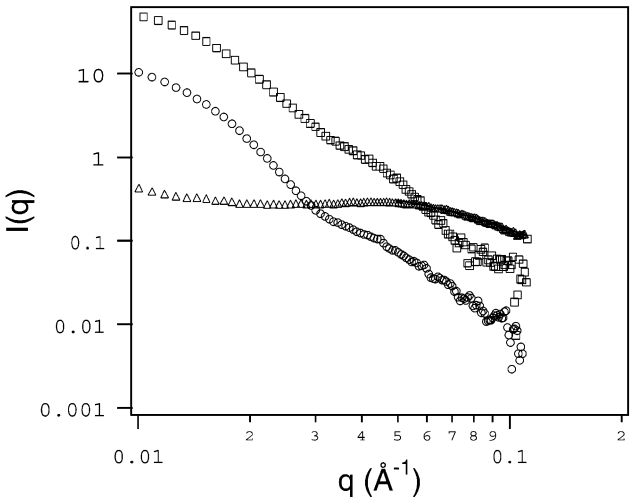


**Figure 6.** Representative SANS profiles for DMAEMA−DEAEMA micelles at 0.001 g/mL (○) and 0.005 g/mL (□) and a DMAEMA homopolymer solution at 0.01 g/mL (△). Guinier (- - -) and Debye (—) fits for the DMAEMA homopolymer solution are also shown.

**3.5. Small-Angle Neutron Scattering.** We performed small-angle neutron scattering (SANS) measurements at the National Institute of Standards and Technology (NIST) Center for Neutron Research (NCNR) in Gaithersburg, MD. Measurements were taken at the 8 m SANS instrument on beamline NG1 as well as on the 30 m instrument on beamline NG3. A 6 m detector distance with a 25.0 cm detector offset from the beam center and a wavelength $\lambda = 6$ Å on the 30 m instrument provided an accessible scattering vector $q$ range of $0.008 < q < 0.11$ Å$^{-1}$. On the 8 m beamline a sample-to-detector distance of 3.6 m, 3.5° detection angle, and incident wavelengths of 5 and 9 Å gave $q$ values spanning $0.008 < q < 0.19$ Å$^{-1}$. Sample cells of 1 mm path length were used. The scattering profiles were corrected for background, empty cell, and solvent scattering, with the appropriate salt solutions in $D_2O$.

Homopolymer and copolymer micelle solutions were prepared as described above, using $D_2O$ (Isotec) as the solvent and titrating with DCl and KOD (Aldrich). Complementary DLS experiments were performed on these same deuterated samples to measure micelle hydrodynamic radii.

Representative SANS scattering profiles for DMAEMA−DEAEMA micelles are shown in Figure 6. Also shown in Figure 6 is the scattering profile for a DMAEMA homopolymer. The scattering profiles show a slight upturn around $0.03 < q < 0.06$ Å$^{-1}$. We believe this upturn could be due to the polyelectrolyte effect which has been observed in the literature.[57,58] Our SANS analysis assumes dilute solutions with no long-range interactions between micelles. As seen in Figure 6, the SANS scattering profiles for 0.001 and 0.005 g/mL copolymer concentrations are qualitativly similar in shape, and the upturn does not increase in intensity with increasing concentration, suggesting that intermicellar interactions are not the cause.

We obtain $R_g$ for both the micelles and homopolymers from a Guinier analysis, using

$$I(q) = I(0)e^{-q^2 R_g^2/3} \quad (4)$$

Representative Guinier plots are shown in Figure 7 for the DMAEMA−DEAEMA micelles at 0.001 g/mL. Homopolymer radii of gyration are also obtained by fitting the homopolymer scattering profile with the Debye equation[59] for the scattering from isolated random coils

$$I(q) = I(0)\left(\frac{2}{x^2}\right)(x - 1 + e^{-x}) \quad (5)$$

Here $x = (qR_g)^2$, and the Debye equation gives $R_g$ values which

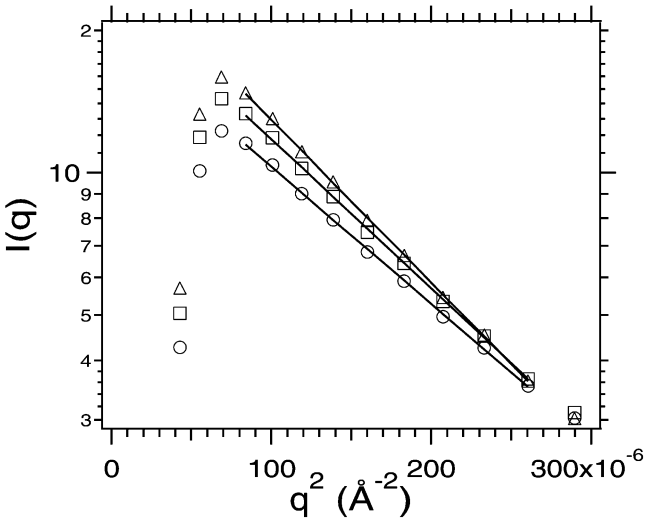


**Figure 7.** Representative Guinier plots for DMAEMA−DEAEMA micelles at 0.006 (○), 0.046 (□), and 0.086 M (△) salt concentrations.

**Table 4. SANS Scattering Length Densities $\rho^N$**

| molecule | $\rho^N \times 10^{-9}$ (cm$^2$) |
|---|---|
| DMAEMA | 8.1 |
| PEO | 6.4 |
| Q-DMAEMA | 11.5 |
| DEAEMA | 5.6 |
| DMAEMA−DEAEMA | 6.9 |
| PEO−DEAEMA | 6.1 |
| Q-DMAEMA−DEAEMA | 8.6 |
| $D_2O$ ($\rho_0^N$) | 63.7 |

we find from our measurements to be slightly larger than those obtained from the Guinier equation. Representative homopolymer Guinier and Debye fits are shown in Figure 6.

From the $y$ intercept of fits to the micelle SANS Guinier plots, we compare $I(0)$ the micelle scattered intensity at $q = 0$ to that of a homopolymer of known molecular weight.[42] We estimate the micelle aggregation numbers $f$ through the ratio of intensities for the homopolymer and micelles given by the Zimm equation, assuming low concentrations such that the second virial term is neglibible, resulting in

$$\frac{M_{w,m}}{M_{w,h}} = \frac{c_h}{c_m}\left(\frac{\rho_h^N - \rho_0^N}{\rho_{bcp}^N - \rho_0^N}\right)^2\left(\frac{\rho_{bcp}}{\rho_h}\right)^2\frac{I(0)_m}{I(0)_h} \quad (6)$$

The subscripts m, bcp, and h correspond to micelle, block copolymer, and homopolymer, respectively, and from eq 6 we obtain $M_{w,m}$ to calculate $f = M_{w,m}/M_{w,bcp}$. Estimates of the scattering length densities $\rho^N$ were calculated by summing over the scattering lengths of the atoms in each molecule[60] and are tabulated in Table 4.

The properties of the homopolymers used to estimate $f$, including PEO, DMAEMA, Q-DMAEMA, and bet-DMAEMA, are tabulated in Table 3. The different homopolymers gave slightly different values for the aggregation number for a given micelle solution, and the reported aggregation numbers are averages over $f$ obtained using different homopolymers. For similar salt concentrations and α, where $C_s \sim 0.04$ M and $\alpha \sim 0.18$, copolymer concentrations of 0.001 and 0.005 g/mL for DMAEMA−DEAEMA micelles give micelle aggregation numbers of 250 and 236, respectively, according to eq 6. The consistency in $f$ for different copolymer concentrations gives validity to the assumption that copolymer concentrations are sufficiently low to neglect the second virial term in the Zimm equation.

The intermediate scattering region in the SANS scattering profile at higher $q$ values provides information about the degree of swelling in the micelle corona, through the Flory exponent $\nu$. The scattering profile approaches an $I(q) \sim q^{1/\nu}$ scaling in the intermediate scattering region, and the data can be fit to obtain $\nu$. The scattering profile can also be plotted as a Kratky plot, as shown in Figure 8 for representative DMAEMA−DEAEMA scattering profiles. In the figure, at $\alpha = 0.37$ the corona is swollen, where the positive slope of the fitted line represents $\nu > 1/2$. Conversely, at $\alpha = 0.19$ the corona shrinks as indicated by the negative slope showing $\nu < 1/2$.

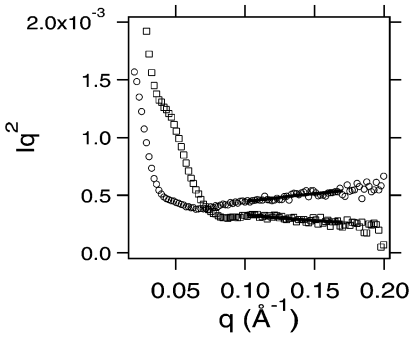


**Figure 8.** Representative SANS scattering Kratky plots for 0.005 g/mL DMAEMA−DEAEMA micelle solutions for $\alpha = 0.37$ (○) and $\alpha = 0.19$ (□). Lines are fits used to obtain values of the Flory exponent $\nu$.

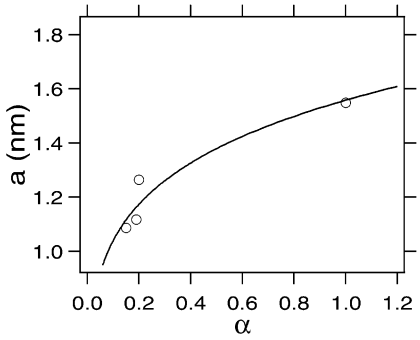


**Figure 9.** Statistical segment length $a$ with varying α. The best fit to data (—) gives $a \sim \alpha^{0.2}$.

There have been studies in the literature where the entire scattering profile is fit to a model form factor.[61−68] We are unable to fit a large portion of our scattering profiles to a simple core−shell model.[64] Contrast matching experiments where the core and corona are observed separately may make this possible.

## 4. Results: pH-Dependent Measurements

**4.1. Weakly Charged Corona: DMAEMA−DEAEMA.** We adjust the fractional charge α in the micelle corona by changing the solution pH. One important parameter that varies with α is the DMAEMA statistical segment length $a$. SANS measurements of the DMAEMA homopolymer $R_g$ provide estimates of $a$ as a function of α. The DMAEMA homopolymer SANS scattering profile in Figure 6 resembles that of a Gaussian coil rather than a wormlike chain. In light of the SANS data, we expect the homopolymer to take on an approximately Gaussian density profile, with $R_g = \sqrt{Na^2}/6$. Using this expression for $R_g$ and the constraint that $Na$ equals the polymer contour length, we calculate the number of statistical segments $N$ and $a$ from Guinier and Debye fits to SANS measurements. A power-law fit through the data for $a$ vs α in Figure 9 gives the dependence $a \sim \alpha^{0.2}$. From the constraint that $Na$ equals the contour length $N \sim \alpha^{-0.2}$.

We measure $R_h$, $R_g$, $f$, and $\nu$ as a function of the solution pH. We present these measurements in terms of the fractional charge α in Figure 10 for 0.005 g/mL

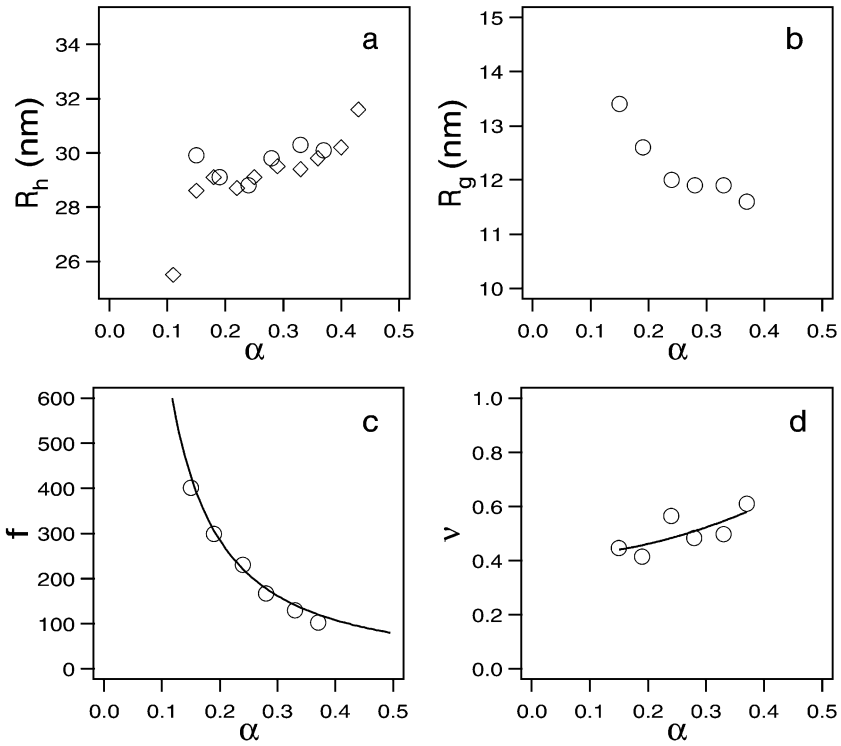


**Figure 10.** $R_h$, $R_g$, $f$, and $\nu$ measurements of DMAEMA−DEAEMA micelles with varying α. Measurements were made for 0.001 (◇) and 0.005 g/mL (○) copolymer solutions. The line in (c) is a power law fit, and the line in (d) is an interpolation to guide the eye. The ionic strength is nearly constant for each copolymer concentration. Error bars for $R_h$ and $R_g$ are generally within the size of the markers.

copolymer concentrations, where the effective amount of KCl added during the titrations ranges from 0.020 to 0.026 M, depending on α. Also included in Figure 10a are $R_h$ measurements obtained for 0.001 g/mL copolymer solutions, with 0.006 M effective KCl added from titrations.

As seen in Figure 10a, the micelle hydrodynamic sizes $R_h$ for the 0.001 g/mL solutions are larger for polymers with larger α due to the swelling of the corona from electrostatic repulsions. The swelling in the corona at higher α can also be observed in Figure 10d, where the Flory exponent $\nu$ increases with increasing α; however, in the 0.005 g/mL solution, $R_h$ decreases with increasing α for $\alpha < 0.24$. An explanation can be found upon observation of the reduction in micelle aggregation number $f$ with charge α in Figure 10c. As the electrostatic repulsions are increased at higher α, fewer copolymer chains aggregate, forming smaller micelles. Hence, the slight decrease in $R_h$ with increasing α for $\alpha < 0.24$ reflects the decrease in $f$ with α. In general, increasing the fractional charge α decreases the aggregation number while at the same time swelling the corona, and these two offsetting effects on the overall micelle size lead to the subtle dependence of $R_h$ on α.

The curve through the aggregation number data in Figure 10c comes from a power-law fit from which the scaling $f \sim \alpha^{-1.5}$ is obtained. As seen in Figure 10b, $R_g$ decreases with increasing α, reflecting its strong dependence on the micelle core. If we assume no solvent swelling in the core, the micelle core size varies as $f^{1/3}$, and so the decrease in $R_g$ with increasing α reflects the decrease in $f$ in Figure 10c.

From the data, we calculate the ratio $R_g/R_h$ as a function of α. The $R_g/R_h$ ratio provides a picture of the degree of swelling in the micelle corona, where low $R_g/R_h$ indicates a swollen corona, due to the fact that $R_g$ is more heavily weighted by the micelle core and $R_h$ increases more rapidly with increased coronal swelling. As seen in Figure 11, $R_g/R_h$ decreases with increasing α, in accord with the earlier discussion that the corona swells as the fractional charge increases. The $R_g/R_h$ ratio for a solid sphere is well-known[69] to be $\sqrt{3/5} \sim 0.77$, and lower $R_g/R_h$ ratios in Figure 11 are expected for micelles, due to the presence of a dense micelle core. Munk and co-workers[70] have shown $R_g/R_h$ for individual micelles to be around 0.4.

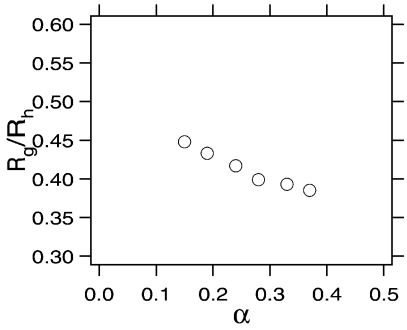


**Figure 11.** $R_g/R_h$ for DMAEMA−DEAEMA micelles with varying α. Lower values of $R_g/R_h$ indicate swelling of the micelle corona.

In Figure 10d $\nu$ decreases below 0.5 at low α, indicating sub-Θ solvent conditions. This apparent sub-Θ scaling in the corona may reflect the interesting molecular structure of these polyacrylate amines.[71] The association between amine and carbonyl groups may cause cyclization with one monomer[71] or intrachain interactions that would appear as an effective segmental attraction.

**4.2. Electrostatically Neutral Corona: PEO−DEAEMA.** The neutral coronal block in PEO−DEAEMA block copolymers should not depend on α,

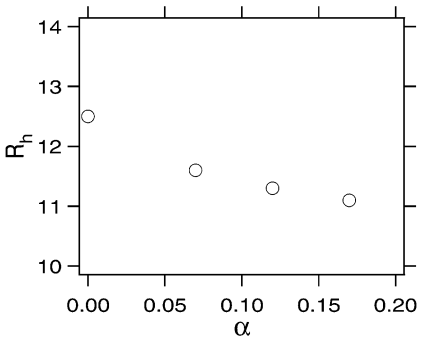


**Figure 12.** $R_h$ for 0.001 g/mL PEO−DEAEMA micelles with varying α.

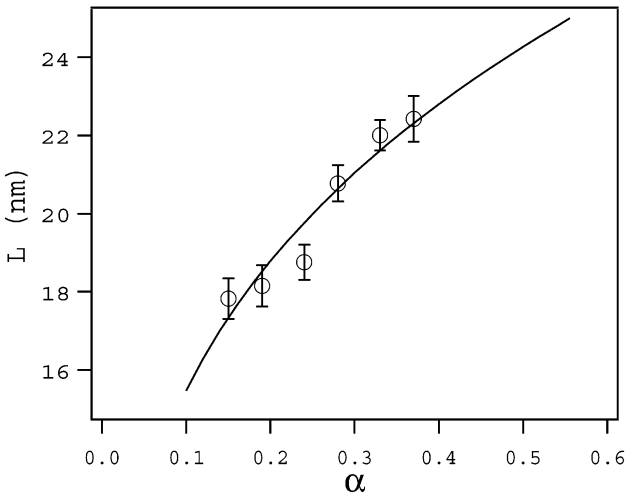


**Figure 13.** Experimentally measured coronal layer thickness $L$ with varying fractional charge α. The fit to the data (—) shows an $\alpha^{0.28}$ scaling.

allowing the study of the α dependence of the DEAEMA core independent of that of the corona. As shown in Figure 12, the PEO−DEAEMA micelle $R_h$ decreases with increasing α due to a decrease in the aggregation number caused by repulsions between core blocks, as seen for the DMAEMA−DEAEMA micelles in Figure 10c. Since the PEO corona is not sensitive to α, the compensating tendency of the corona to swell with increasing α is absent.

**4.3. Comparison with Theoretical Models.** From the data in Figure 10 the corona thickness $L$ is calculated by subtracting the overall micelle radius $R_h$ from the core radius $R_c$. In this calculation of $L$ we assume that the hydrodynamic radius $R_h$ from our DLS measurements is representative of the actual micelle radius. $R_c$ is calculated from the measured aggregation numbers in Figure 10c, assuming that the DEAEMA blocks form a densely packed core with a density equal to that of bulk DEAEMA. From $R_c$ and $f$ the grafting density $\sigma$ can also be calculated. From the $f \sim \alpha^{-1.5}$ dependence found from the experimental measurements we calculate the scalings $R_c \sim \alpha^{-0.5}$ and $\sigma \sim \alpha^{-0.5}$. The measured $L$ dependence on α is compared to that predicted by theoretical models from the literature in order to gain additional insight into the nature of the charging. Shown in Figure 13 are the measured corona thicknesses $L$, with a power law fit, giving the scaling $L \sim \alpha^{0.28}$.

As described earlier, the osmotic and salted regimes correspond to low and high ionic strengths, respectively. The amount of salt added during micelle preparation decreases from 0.026 to 0.020 M, while the counterion concentration increases from 0.005 to 0.011 M with increasing α. The amount of added salt is comparable to the counterion concentration, suggesting that the micelle corona is somewhere between the osmotic and salted regimes. Typically, $R_c \sim 10$ nm and $R_h \sim 30$ nm, such that models for a curved interface are more appropriate than for a flat interface.

From Table 1, the $L \sim \alpha^{1/2}Na$ scaling for quenched polyelectrolyte brushes suggests an $\alpha^{1/2}$ scaling for $L$, in reasonable agreement with the data. Our starlike micelle model with electrostatic blobs also predicts an $\alpha^{1/2}$ scaling. The model of Borisov and Zhulina[72] for the annealed salted brush at a spherical interface might be expected to better describe the DMAEMA−DEAEMA micelles. As seen in Table 2, the model describes an $L \sim N^3\alpha_b f^{-1}(C_H^* + C_s)a^4$ scaling. As described earlier, $a \sim \alpha^{0.2}$ and $N \sim \alpha^{-0.2}$ according to Figure 9 and $f \sim \alpha^{-1.5}$ according to Figure 10c. These scalings of $a$, $N$, and $f$ can be substituted into $L \sim N^3\alpha_b f^{-1}(C_H^* + C_s)a^4$ to obtain an overall α dependence $L \sim \alpha^{2.7}$, giving a much stronger α dependence than the data show. Borsov and Zhulina also explain that at high enough added salt concentrations the annealed brush behaves as a quenched salted brush because α within the brush approaches the bulk value $\alpha_b$ at high salt concentrations.[72] Borisov and Zhulina's model for quenched salted brushes at spherical interfaces in Table 1 gives $L \sim N^{3/5}f^{1/5}\alpha^{2/5}(C_s a^3)^{-1/5}a$. Substituting the α dependences of $N$, $a$, and $f$ into this scaling gives an overall scaling $L \sim \alpha^{0.3}$, in close agreement with the experimental $\alpha^{0.28}$ scaling.

The close agreement of the quenched salted brush model with the experimental data indicates that $\alpha \sim \alpha_b$ inside the micelle corona. The titration data in Figure 3 support this, in that the experimental titration data for the micelles are in close agreement with the theoretically predicted titration curves which assume $\alpha \sim \alpha_b$. Groenewegen et al. have measured the micelle radius of polystyrene-*block*-poly(acrylic acid) (PS−PA) copolymers as a function of α, where the core radius and $f$ are constant.[39] They have found the micelle size to scale as $\alpha^{2/5}$, which is similar to our results. In their analysis they assume $a$ is not dependent on α, and their results are in close agreement with the theory of Borisov and Zhulina.

## 5. Results: Dependence on Ionic Strength

**5.1. Weakly Charged Corona: DMAEMA−DEAEMA.** The ionic strength dependence of the DMAEMA−DEAEMA micelle hydrodynamic radius $R_h$, radius of gyration $R_g$, and aggregation number $f$ is shown in Figure 14. Results from 0.001 g/mL copolymer concentrations are shown, with the dependence on salt added both before and after micellization. Small amounts of salt are inevitably formed during titration; the effective amount added in these experiments is 0.006 M for a 0.001 g/mL copolymer concentration. The ordinate of the graphs in Figure 14 accounts for the total salt concentration. The DMAEMA−DEAEMA copolymers were titrated to form micelles at constant fractional charges α of 0.17.

As seen in Figure 14a, when salt is added prior to the formation of micelles, $R_h$ remains relatively constant; however, as also shown in Figure 14a, when salt is added after micelle formation, $R_h$ decreases with the addition of salt. We expect the addition of salt to screen

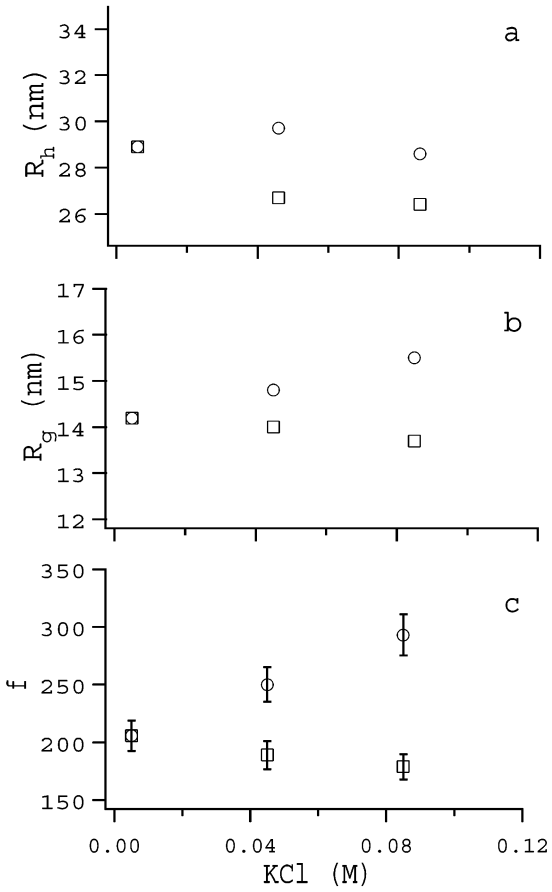


**Figure 14.** DMAEMA−DEAEMA micelle hydrodynamic radius $R_h$, radius of gyration $R_g$, and aggregation number $f$ as a function of salt added before (○) and after (□) micellization. The data are for 0.001 g/mL solutions, with $\alpha \sim 0.17$. Error bars for $R_h$ and $R_g$ are generally within the size of the markers.

the electrostatic repulsions in the charged corona, leading to a smaller corona thickness, as observed in the decrease in $R_h$ when salt is added after the formation of micelles. Prior to micellization, both blocks of the copolymers are highly charged; thus, electrostatic repulsions work against the formation of micelles during the titrations. Addition of salt before micellization screens the electrostatic repulsions, allowing larger numbers of chains to aggregate to form larger micelles during the titrations. This increase in the aggregation number $f$ is seen in Figure 14c. Hence, when added prior to the formation of micelles, the salt tends to cause larger micelles to form, while at the same time shrinking the micelle corona. These two offsetting effects cause the weak dependence of $R_h$.

Measurements of the DMAEMA−DEAEMA radius of gyration $R_g$ are shown as a function of added salt in Figure 14b. When salt is added after micellization, $R_g$ decreases with added salt, following the same trend as the decrease in $R_h$. When salt is added before micellization, we find that $R_g$ increases with added salt, in contrast with the weak $R_h$ dependence. The competing effects of the increasing aggregation number and the decrease in the corona thickness have opposite effects on the micelle size, but since $R_g$ is more heavily weighted toward the micelle core, it more directly reflects the increased aggregation number in Figure 14c.

Aggregation numbers for DMAEMA−DEAEMA micelles are plotted in Figure 14c for salt added before and after micellization. As discussed above, adding salt

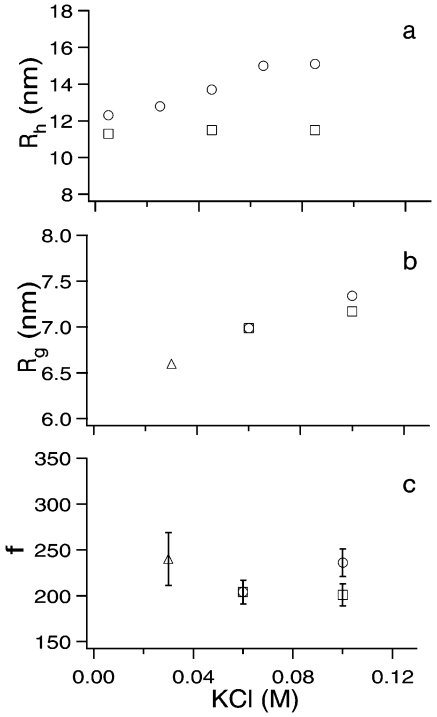


**Figure 15.** PEO−DEAEMA hydrodynamic radius $R_h$, radius of gyration $R_g$, and aggregation number $f$ vs ionic strength data for salt added before (○) and after (□) micellization at 0.001 g/mL for $R_h$ and 0.01 g/mL for $R_g$ and $f$ measurements. Micelles at 0.005 g/mL (△) were also studied. $\alpha = 0$ for all solutions. Error bars for $R_h$ and $R_g$ are generally within the size of the markers.

before micellization screen electrostatic repulsions between chains allowing the formation of larger numbers of chains to come together to form micelles with larger $f$. When salt is added after micelle formation, the aggregation number is relatively constant, as seen in Figure 14c.

The difference in $R_h$, $R_g$, and $f$ depending on the order of salt addition suggests that the micelles are nonequilibrium structures. Micelle formation and breakup upon addition of base or acid occurs extremely quickly, on the time scale of milliseconds. The fast micellization kinetics may impede equilibration. The deviation in the $R_h$, $R_g$, and $f$ behavior persists even weeks after sample preparation, suggesting that rearrangement of chains between micelles is extremely slow due to strong hydrophobic attractions which cause the micelle core to take on a glassy nature, as observed by Groenewegen et al.[39,40] and Van der Maarel et al.[36]

**5.2. Electrostatically Neutral Corona: PEO−DEAEMA.** The PEO−DEAEMA copolymer allows us to study the effect of ionic strength on the core DEAEMA block separately. The $R_h$, $R_g$, and $f$ dependence on salt are shown in Figure 15 at the concentrations and conditions described in the figure caption. The copolymers were titrated with sufficient base such that the DEAEMA core $\alpha = 0$.

Because the PEO block is electrostatically neutral, electrostatic screening in the corona is probably not responsible for the salt-dependent behavior. As seen in Figure 15a, when salt is added after micelle formation, the decrease in $R_h$ seen for DMAEMA−DEAEMA is absent because of the electrostatically neutral PEO corona. When salt is added prior to titration, $R_h$ increases with added salt since the salt screens the electrostatic repulsions between DEAEMA blocks, al-

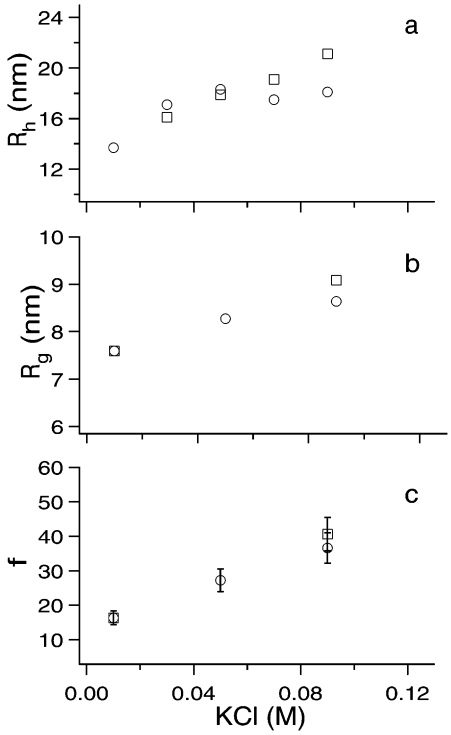


**Figure 16.** Q-DMAEMA−DEAEMA hydrodynamic radius $R_h$, radius of gyration $R_g$, and aggregation number $f$ vs ionic strength data for salt added before (○) and after (□) micellization. The data are for 0.005 g/mL solutions, with $\alpha = 0$ in the DEAEMA blocks. Error bars for $R_h$ and $R_g$ are generally within the size of the markers.

lowing larger numbers of copolymers to aggregate into the core of larger micelles. The competing effect of the salt causing the DMAEMA corona to shrink is absent in the PEO corona, such that the PEO−DEAEMA $R_h$ reflects the increase in $f$.

The $R_g$ data for PEO−DEAEMA micelles shown in Figure 15b follow the same trend for salt added before micellization as seen in DMAEMA−DEAEMA micelles. For salt added after micellization, $R_g$ does not decrease since, in contrast to the DMAEMA−DEAEMA micelles, the PEO micelle corona is uncharged.

PEO−DEAEMA aggregation numbers shown in Figure 15c support the $R_h$ and $R_g$ results. When salt is added prior to micellization, the aggregation number increases due to electrostatic screening of the core forming DEAEMA blocks. When salt is added after micellization, the aggregation number remains relatively constant.

**5.3. Highly Charged Corona: Q-DMAEMA−DEAEMA.** We study the dependence of the Q-DMAEMA−DEAEMA copolymer on ionic strength, where the micelle corona is a strong polyelectrolyte. The copolymers are titrated such that $\alpha \sim 0$ for the DEAEMA block to form micelles. The Q-DMAEMA block forming the micelle corona remains fully charged at $\alpha \sim 1$ and is independent of the solution pH.

In these micelles, both $R_h$ and the apparent aggregation number increase with ionic strength, whether salt is added prior to or after micellization, as seen in Figure 16a,c. This behavior contrasts with the DMAEMA−DEAEMA and the PEO−DEAEMA behavior, and the difference is most certainly caused by the highly charged Q-DMAEMA corona. As salt is added and screens the electrostatic repulsions, additional unimers are incorporated into the micelles to increase their size. These

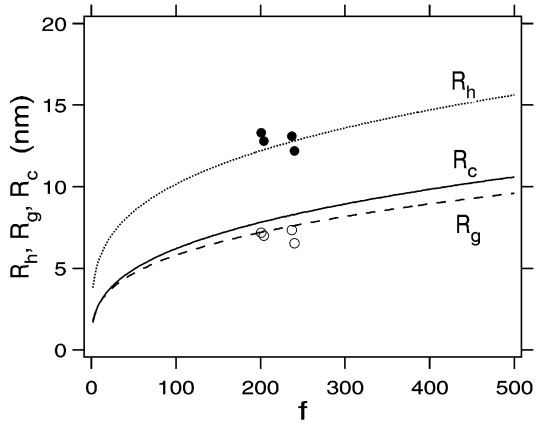


**Figure 17.** Experimentally measured $R_h$ (●) and $R_g$ (○) as a function of $f$ for PEO−DEAEMA micelles compared with the starlike micelle model $R_c$ (—), $R_g$ (- - -), and $R_h$ (···).

**Table 5. Parameters Used in the Starlike Micelle Model**

| copolymer | $a$ (nm) | $V_s$ (nm$^3$) | $\rho_c$ (nm$^{-3}$) | $\nu$ | $N_c$ | $N_s$ |
|---|---|---|---|---|---|---|
| DMAEMA−DEAEMA | 1.2 | 0.69 | 3.41 | 0.5 | 94 | 26 |
| PEO−DEAEMA | 0.61 | 0.09 | 3.41 | 0.6 | 34 | 33 |

small, highly charged micelles are able to rearrange even when salt is added after micellization, such that the dependence on $f$ is the same in both cases.

The trends for $R_g$ with ionic strength follow those in $R_h$, as seen in Figure 16, again whether salt is added prior to or after micellization. As $R_g$ favors the core radius, the increase of $R_g$ with salt reflects the increase in aggregation number.

**5.4. Comparison with Theoretical Models. 5.4.1. Starlike Micelle Model.** We start by examining the starlike micelle model for predictions of $R_h$ and $R_g$ with varying $f$ for the simplest case of electrostatically neutral micelles. As described earlier, SANS experiments were performed on DMAEMA, Q-DMAEMA, and PEO homopolymers to obtain the statistical segment $a$ in the micelle corona. For the DMAEMA homopolymer, an average $a$ at $\alpha \sim 0.2$ was used to match the conditions where the DMAEMA−DEAEMA micelle $R_g$ and $R_h$ were measured. From $a$ we calculate volume per segment $V_s$ and the number of segments $N_s$ per chain in the corona. The core DEAEMA block is considered to be densely packed, and thus the definition of the statistical segment in the micelle core is irrelevant. NMR studies have indicated dehydration of the micelle core,[73] so the core density, $\rho_c$, comes directly from the DEAEMA core monomer molecular weight and density. Using SANS Kratky plots as a guide, 0.5 and 0.6 were used for the Flory exponent $\nu$ for DMAEMA and PEO, respectively. We use these parameters summarized in Table 5 to calculate $R_c$, $R_g$, and $R_m$ from the starlike micelle model. The SANS neutron scattering length densities $\rho^N$ used in the model to calculate $R_g$ are tabulated in Table 4.

The experimentally measured PEO−DEAEMA $R_h$ and $R_g$ data from Figure 15 are plotted in Figure 17 as a function of the aggregation number $f$, along with curves predicted by the starlike model. We find excellent quantitative agreement between the data and the model, and the $R_g/R_h$ values of ∼0.55 for the data are comparable to the values of ∼0.6 from the model.

The DMAEMA−DEAEMA $R_h$ and $R_g$ data from Figure 14 do not agree well with predictions from the starlike model, as shown in Figure 18. Also included in

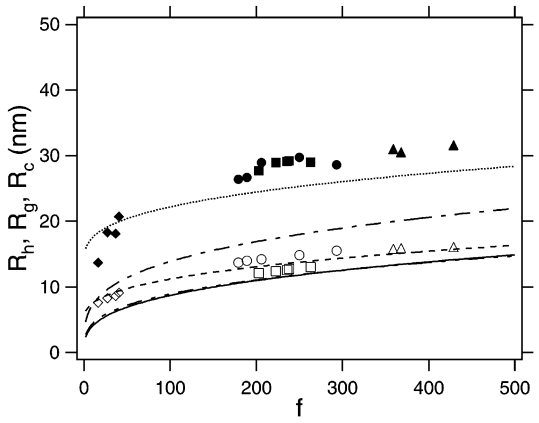


**Figure 18.** Experimental $R_h$ (filled) and $R_g$ (open) measurements as a function of $f$ for 0.001 (○), 0.005 (□), and 0.0075 g/mL (△) DMAEMA−DEAEMA micelle solutions. Also included are results for Q-DMAEMA−DEAEMA micelles (◇). Results are compared with the starlike micelle model predictions for $R_c$ (—), $R_g$ (— - - —), and $R_h$ (— - —), as well as for the electrostatic blob model for $R_g$ (- - -) and $R_h$ (•••).

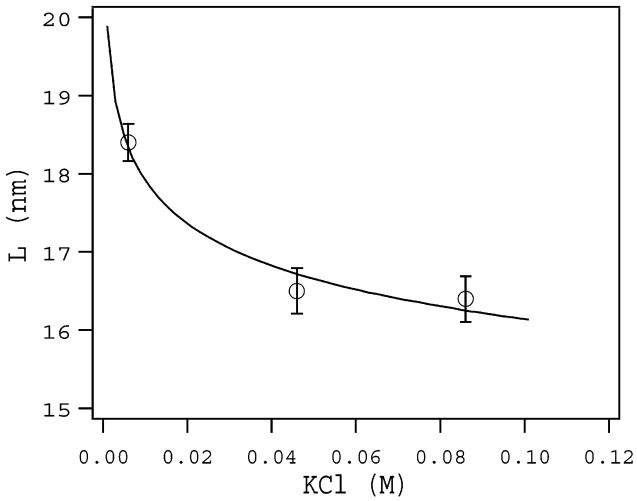


**Figure 19.** Experimentally measured coronal layer thickness $L$ with varying salt concentration $C_s$. The fit to the data (—) gives a $C_s^{-0.05}$ scaling.

Figure 18 are Q-DMAEMA−DEAEMA data from Figure 16. Quantitatively, $R_g$ is somewhat underpredicted, while $R_h$ is greatly underpredicted by the model. The closer agreement between the measured and predicted $R_g$ values indicates that the model does reasonably well in predicting the core size, which is more heavily weighted in $R_g$. The disagreement between the model and experimental results is not surprising, as the model was developed for neutral micelles. The charges in the micelle corona alter the blob picture in the corona, such that the model is inadequate to describe the DMAEMA−DEAEMA $R_g$ and $R_h$ behavior.

The disagreement between the DMAEMA−DEAEMA data and the starlike micelle model motivated us to develop the starlike micelle model with electrostatic blobs described in the Theory section. Shown in Figure 18 are predictions of $R_m$ and $R_g$ from the electrostatic blob model. As seen in Figure 18, this fairly simple model does well describing the data and predicts $R_g/R_h \sim 0.55$, a significant improvement over the starlike micelle model. The hydrodynamic micelle radius $R_h$ is probably slightly larger that the actual radius $R_m$, and this is reflected in Figure 18 where $R_h$ is slightly underpredicted by the starlike model with electrostatic blobs.

**5.4.2. Models for Ionic Strength Dependence of Polyelectrolyte Brushes.** The micelle corona thickness $L$ is calculated as $R_h - R_c$, as described earlier. Data for the salt added after micellization case from Figure 14 were used to calculate $L$, and $L$ is plotted as a function of $C_s$ in Figure 19. As seen in Tables 1 and 2, the models of Zhulina and co-workers,[28] Pincus,[19] and Lyatskaya and co-workers[29] predict $L$ to scale as $C_s^{-1/3}$, while Argillier and Tirrell[20] developed a model in which $L \sim C_s^{-2/3}$. The model of Hariharan and co-workers[25] gives the scaling $L \sim C_s^{-1/6}$ for a brush at a planar interface and for a highly curved interface $L \sim C_s^{-1/10}$. In addition, Borisov and Zhulina[72] predict $L \sim C_s^{-1/5}$ for a brush at a highly curved interface. The models mentioned above also include $\sigma$ and $R_c$ dependences on $L$, but $\sigma$ and $R_c$ are essentially constant for the data in Figure 19. As seen in the figure, the data fit a $C_s^{-0.05}$ scaling, which is weaker than predicted by the models. We do not expect the $C_s^{-1/3}$, $C_s^{-2/3}$, and $C_s^{-1/6}$ scalings for polyelectrolyte brushes at a planar surface to fit since the DMAEMA−DEAEMA micelle corona is a brush on a curved interface with $R_c \sim 10$ nm and $L \sim 18$ nm. The $C_s^{-1/10}$ scaling predicted for a brush at a spherical interface is still too strong but most closely agrees with the limited experimental data.

In the literature, Hariharan et al.[25] have experimentally measured hydrodynamic radii of poly(*tert*-butylstyrene)-*block*-poly(styrenesulfonate) (PtBS−PSS) micelles as well as PtBS−PSS copolymers adsorbed onto polystyrene particles and have found $R_h \sim C_s^{-0.11}$ and $R_h \sim C_s^{-0.15}$ for PtBS−PSS micelles and $R_h \sim C_s^{-0.18}$ for PtBS−PSS adsorbed onto particles. These scalings are in agreement with their theoretical scalings. Van der Maarel et al.[36] have measured the radius for polystyrene-*block*-poly(acrylic acid) (PS−PA) copolymer micelles to scale as $C_s^{-1/5}$, which is in agreement with the theory of Borisov and Zhulina. Wesley et al.[52] have measured hydrodynamic radii of 2-(dimethylamino)ethyl methacrylate-*block*-methyl methacrylate (DMAEMA−MMA) copolymers adsorbed onto PMMA latex spheres and have found $R_h \sim C_s^{-1/3}$, in agreement with the theories of Zhulina et al., Pincus, and Lyatskaya et al. The variation of these experimental results is probably related to variations of the degree of curvature of the interface. All of these experimental results show a stronger salt dependence than our results. One possible explanation for the weak salt dependence in Figure 19 is that $\alpha \sim 0.17$ for these micelles, such that the micelle coronae are weakly charged compared to those studied in the literature, leading to a weaker dependence on ionic strength.

## 6. Conclusions

Dynamic light scattering and small-angle neutron scattering were used to characterize the structural properties of polyelectrolyte micelles with varying fractional charge $\alpha$ and ionic strength. Two opposing effects on the overall micelle size are the aggregation number $f$ and the degree of swelling in the micelle corona. Increasing $\alpha$ tends to decrease $f$ and increase the coronal swelling, due to the increase in electrostatic repulsions, while increasing the ionic strength has the opposite effect on $f$ and the swelling due to electrostatic screening. Both effects are seen in the DMAEMA−DEAEMA micelles, due to the pH-sensitive $\alpha$ in both the core and coronal blocks. Studies of the PEO−DEAEMA micelles

illustrate the effect of charge and salt on the core block only, and the micelle structure is found to be governed by *f*, without the effect of the coronal swelling. The highly charged Q-DMAEMA−DEAEMA micelles follow the salt dependence of DMAEMA−DEAEMA micelles, except that the Q-DMAEMA−DEAEMA micelles are able to rearrange after the formation of micelles, due to their high charge and small size. We compare the experimental data to theoretical models and find that the DMAEMA−DEAEMA weakly charged micelle corona can be described by an electrostatic blob picture.

**Acknowledgment.** This work was supported by the Center for Polymer Interfaces and Macromolecular Assemblies through the National Science Foundation MRSEC program (DMR 9808677). J.A.P. and A.P.G. acknowledge the support of the Stanford Synchrotron Radiation Laboratory through the Department of Energy Contract DE-AC03-76SF00515. We acknowledge the support of the National Institute of Standards and Technology, US Department of Commerce, for providing the facilities used in the neutron scattering experiments described in this paper.

## References and Notes

(1) Tuzar, Z.; Kratochvil, P. *Adv. Colloid Interface Sci.* **1976**, *6*, 201.
(2) Halperin, A.; Tirrell, M.; Lodge, T. P. *Adv. Polym. Sci.* **1992**, *100*, 31.
(3) Zhang, L.; Eisenberg, A. *Science* **1995**, *268*, 1728.
(4) Zhang, L.; Yu, K.; Eisenberg, A. *Science* **1996**, *272*, 1777.
(5) Gast, A. P. *Langmuir* **1996**, *12*, 4060.
(6) Vagberg, L. J. M.; Cogan, K. A.; Gast, A. P. *Macromolecules* **1991**, *24*, 1670.
(7) Cogan, K. A.; Gast, A. P. *Macromolecules* **1991**, *24*, 6512.
(8) Cogan, K. A.; Gast, A. P. *Macromolecules* **1990**, *23*, 745.
(9) Farinha, J. P. S., d'Oliveira, J. M. R.; Martinho, J. M. G.; Xu, R.; Winnik, M. A. *Langmuir* **1998**, *14*, 2291.
(10) Cogan, K. A.; Leermakers, F. A. M.; Gast, A. P. *Langmuir* **1992**, *8*, 429.
(11) Daoud, M.; Cotton, J. P. *J. Phys.* (*Paris*) **1982**, *43*, 531.
(12) Noolandi, J.; Hong, K. M. *Macromolecules* **1983**, *16*, 1443.
(13) Marques, C.; Joanny, J. F.; Leibler, L. *Macromolecules* **1988**, *21*, 1051.
(14) Dan, N.; Tirrell, M. *Macromolecules* **1992**, *25*, 2890.
(15) Wijmans, C. M.; Zhulina, E. B. *Macromolecules* **1993**, *26*, 7214.
(16) Grest, G. S.; Kremer, K.; Witten, T. A. *Macromolecules* **1987**, *20*, 1376.
(17) Witten, T. A.; Pincus, P. A. *Macromolecules* **1986**, *19*, 2509.
(18) Misra, S.; Varanasi, S.; Varanasi, P. P. *Macromolecules* **1989**, *22*, 4173.
(19) Pincus, P. *Macromolecules* **1991**, *24*, 2912.
(20) Argillier, J. F.; Tirrell, M. *Theor. Chim. Acta* **1992** *82*, 343.
(21) Dan, N.; Tirrell, M. *Macromolecules* **1993**, *26*, 4310.
(22) Borisov, O. V. *J. Phys. II* **1996**, *6*, 1.
(23) Shusharina, N. P.; Nyrkova, I. A.; Khokhlov, A. R. *Macromolecules* **1996**, *29*, 3167.
(24) Biver, C.; Hariharan, R.; Mays, J.; Russel, W. B. *Macromolecules* **1997**, *30*, 1787.
(25) Hariharan, R.; Biver, C.; Mays, J.; Russel, W. B. *Macromolecules* **1998**, *31*, 7506.
(26) Zhulina, E. B.; Borisov, O. V. *Macromolecules* **1996**, *29*, 2618.
(27) Israels, R.; Leermakers, F. A. M.; Fleer, G. J. *Macromolecules* **1994**, *27*, 3087.
(28) Zhulina, E. B.; Birshtein, T. M.; Borisov, O. V. *Macromolecules* **1995**, *28*, 1491.
(29) Lyatskaya, Y. V.; Leermakers, F. A. M.; Fleer, G. J.; Zhulina, E. B.; Birshtein, T. M. *Macromolecules* **1995**, *28*, 3562.
(30) Szczubialka, K.; Ishikawa, K.; Morishima, Y. *Langmuir* **1999**, *15*, 454.
(31) Prochazka, K.; Martin, T. J.; Munk, P.; Webber, S. E. *Macromolecules* **1996**, *29*, 6518.
(32) Guenoun, P.; Davis, H. T.; Tirrell, M.; Mays, J. W. *Macromolecules* **1996**, *29*, 3965.
(33) Baines, F. L.; Armes, S. P.; Billingham, N. C.; Tuzar, Z. *Macromolecules* **1996**, *29*, 8151.
(34) Guenoun, P.; Schlachli, A.; Sentenac, D.; Mays, J. W.; Benattar, J. J. *Phys. Rev. Lett.* **1995**, *74*, 3628.
(35) An, S. W.; Thirtle, P. N.; Thomas, R. K.; Baines, F. L.; Billingham, N. C.; Armes, S. P.; Penfold, J. *Macromolecules* **1999**, *32*, 2731.
(36) van der Maarel, J. R. C.; Groenewegen, W.; Egelhaaf, S. U.; Lapp, A. *Langmuir* **2000**, *16*, 7510.
(37) Baines, F. L.; Billingham, N. C.; Armes, S. P. *Macromolecules* **1996**, *29*, 3416.
(38) Biesalski, M.; Rifihe, J.; Johannsmann, D. *J. Chem. Phys.* **1999**, *111*, 7029.
(39) Groenewegen, W.; Egelhaaf, S. U.; Lapp, A.; van der Maarel, J. R. C. *Macromolecules* **2000**, *33*, 3283.
(40) Groenewegen, W.; Lapp, A.; Egelhaaf, S. U.; van der Maarel, J. R. C. *Macromolecules* **2000**, *33*, 4080.
(41) Martin, T. J.; Prochdzka, K.; Munk, P.; Webber, S. E. *Macromolecules* **1996**, *29*, 6071.
(42) Lee, A. S.; Biitin, V.; Armes, S. P.; Gast, A. P. *Macromolecules* **1999**, *32*, 4302.
(43) Selb, J.; Gallot, Y. Ionic Block Copolymers. In *Developments in Block Copolymers*-2; Goodman, I., Ed.; Elsevier Applied Science Publishers: New York, 1985; pp 27−96.
(44) Yatvin, M. B.; Kreutz, W.; Horwitz, B. A.; Shinitzky, M. *Science* **1980**, *210*, 1253.
(45) Seki, K.; Tirrell, D. A. *Macromolecules* **1984**, *17*, 1692.
(46) Thomas, J. L.; Tirrell, D. A. *Acc. Chem. Res.* **1992**, *25*, 336.
(47) Mosler, R.; Hatton, T. A. *Curr. Opin. Colloid Interface Sci.* **1996**, *1*, 540.
(48) Biitiin, V.; Billingham, N. C.; Armes, S. P. *Chem. Commun.* **1997**, 671.
(49) Vamvakaki, M.; Billingham, N. C.; Armes, S. P. *Macromolecules* **1999**, *32*, 2088.
(50) Lowe, A. B.; Billingham, N. C.; Armes, S. P. *Chem. Commun.* **1996**, 1555.
(51) Biitiin, V.; Bennett, C. E.; Vamvakaki, M.; Lowe, A.; Billingham, N. C.; Armes, S. P. *J. Mater. Chem.* **1997**, *7*, 1693.
(52) Wesley, R. D.; Cosgrove, T.; Thompson, L.; Armes, S. P.; Billingham, N. C.; Baines, F. L. *Langmuir* **2000**, *16*, 4467.
(53) Oxtoby, D. W.; Nachtrieb, N. H. *Principles of Modern Chemistry*; Saunders College Publishing: Philadelphia, 1986.
(54) Provencher, S. W.; Hendrix, J.; DeMaeyer, L.; Paulussen, N. *J. Chem. Phys.* **1978**, *69*, 4273.
(55) Provencher, S. W. *Comput. Phys. Commun.* **1982**, *27*, 213.
(56) Bartlett, P.; Ottewill, R. H. *J. Phys. Chem.* **1992**, *96*, 3306.
(57) Borsali, R.; Nguyen, H.; Pecora, R. *Macromolecules* **1998**, *31*, 1548.
(58) Ermi, B. D.; Amis, E. J. *Macromolecules* **1998**, *31*, 7378.
(59) Debye, P. *J. Phys. Colloidal Chem.* **1947**, *51*, 18.
(60) Higgins, J. S.; Maconnachie, A. Neutron Scattering from Macromolecules in Solution. In *Polymers in Solution*; Forsman, W. C., Ed.; Plenum Press: New York, 1986; pp 183−238.
(61) Dozier, W. D.; Huang, J. S.; Fetters, L. J. *Macromolecules* **1991**, *24*, 2810.
(62) Stellbrink, J.; Willner, L.; Jucknischke, O.; Richter, D.; Lindner, P.; Fetters, L. J.; Huang, J. S. *Macromolecules* **1998**, *31*, 4189.
(63) Pedersen, J. S.; Egelhaaf, S. U.; Schurtenberger, P. *J. Phys. Chem.* **1995**, *99*, 1299.
(64) Poppe, A.; Willner, L.; Allgaier, J.; Stellbrink, J.; Richter, D. *Macromolecules* **1997**, *30*, 7462.
(65) Nakano, M.; Matsuoka, H.; Yamaoka, H.; Poppe, A.; Richter, D. *Macromolecules* **1999**, *32*, 697.
(66) Schurtenberger, P.; Jerke, G.; Cavaco, C.; Pedersen, J. S. *Langmuir* **1996**, *12*, 2433.
(67) Jerke, G.; Pedersen, J. S.; Egelhaaf, S. U.; Schurtenberger, P. *Langmuir* **1998**, *14*, 6013.
(68) Won, Y.-Y.; Davis, H. T.; Bates, F. S. *Science* **1999**, *283*, 960.
(69) Mallamace, F.; Micali, N. Low Angle Light Scattering and Its Applications. In *Light Scattering*: *Principles and Development*; Brown, W., Ed.; Clarendon Press: Oxford, 1996; pp 381−438.
(70) Qin, A.; Tian, M.; Ramireddy, C.; Webber, S. E.; Munk, P.; Tuzar, Z. *Macromolecules* **1994**, *27*, 120.
(71) Přádný, M.; Ševčík, S. *Makromol. Chem.* **1985**, *186*, 111.
(72) Borisov, O. V.; Zhulina, E. B. *Eur. Phys. J. B* **1998**, *4*, 205.
(73) Bütün, V.; Armes, S. P.; Billingham, N. C. *Polymer* **2001**, *42*, 5993.
(74) Odijk, T.; Houwaart, A. C. *J. Polym. Sci., Polym. Phys. Ed.* **1978**, *16*, 627.
(75) Fixman, M. *J. Phys. Chem.* **1990**, *15*, 6283.

MA0114842